Regular Article

PHYSICAL CHEMISTRY RESEARCH
Published by the
Iranian Chemical Society
www.physchemres.org
info@physchemres.org

Phys. Chem. Res., Vol. 11, No. 2, 315-326, June 2023
DOI: 10.22036/pcr.2022.335182.2065

RSM Optimized Adsorption of Eriochrome Black T Dye onto Alumina Nanoprticles: Isotherm and Kinetics Studies

A.M. Bello*, N.A. Muhammad and A. Hamisu

Department of Chemistry, Faculty of Sciences, Kano University of Science and Technology Wudil, PMB 3244, Kano State, Nigeria

(Received 25 March 2022, Accepted 17 June 2022)

Nanoparticles materials with proper structural properties are excellent candidates for the remediation of wastewater. In this study, mesoporous gamma-alumina was synthesized from kaolin using polyoxyethylene (40) stearate (PS) surfactant. The XRD diffractogram of the alumina revealed broad peaks that indicated the small crystallites. The FTIR spectrum indicated that the alumina possessed both tetrahedral and octahedral structure. The surface area, average pore diameter, and pore volume obtained from the N_2-sorption study were 76.0 m^2 g^{-1}, 4.4 nm, and 0.14 cm^3 g^{-1}, respectively. The XRF result revealed up to 98% Al_2O_3 composition, indicating very high purity of the alumina. The alumina (Nano-Al) was used for the adsorption of Eriochrome Black T dye and the process was optimized using RSM analysis by the Central Composite Design model. From the optimization results, the model's R^2 (0.8736) value implies that 87.36% of the dye removal could be due to the variation in the independent variable. The F-value of 7.68 implies the model is significant. Consequently, 98.2% dye removal was achieved under the optimum conditions. This may be attributed to the enhanced structural properties of the Nano-Al. The experimental data were best fitted to Langmuir isotherm, and the adsorption kinetics data were fitted to the pseudo-second-order model.

Keywords: Mesoporous alumina, Adsorption, Optimization, Dye

INTRODUCTION

Water is an essential element for all living beings, constituting about 71% of the earth's surface. However, only about 1% of this represents the inland waters meant for consumption. Although the total abundance of water is not a problem, the problem is water availability at the right place, at the right time, and in the right form. Water is thus of great importance and is required for all life processes on earth. Water, and particularly the movement of water, is also important as it contains much of the pollution that humans generate [1].

Industrial effluents frequently pollute the sources of water supplies. Today, synthetic dyes are used extensively for textile dyeing and as additives to petroleum products. There are more than 10000 different types of dyes and pigments available commercially and about 10-15% of dyes are used in the effluent during the dyeing process [2]. More than 9000 types of dyes have been incorporated into the color index and environmental regulations in most countries; these regulations made it mandatory to decolorize dye wastewater before discharge [3]. Textile effluents are highly visible to the human eye, capturing the attention of both public and the authorities. It has received great attention, due to its physiological impact on the population [4].

Synthetic dyes are difficult to eliminate under aerobic conditions and are frequently decomposed into carcinogenic aromatic amines under anaerobic conditions; hence, they are considered highly treacherous. Besides, these dyes are not easily removed using chemical coagulation due to their high solubility in water [5]. Eriochrome Black T (EBT) is an azo dye that falls under the category of anionic dyes used in complexometric titrations and for dyeing silk, wool, and nylon. It is not often degraded or removed by conventional

*Corresponding author. E-mail: muhbaf70@yahoo.com

physical, chemical, traditional aerobic treatment, and biological oxidative processes. Thus, the removal of EBT is a challenging problem to address.

The main water contamination response techniques include a variety of filters, chemical dosing, reverse osmosis, gravity separation, ultra-filtration, micro-filtration, biological processes, air flotation, membrane bioreactor, chemical coagulation, electro-coagulation, and electro-flotation. However, adsorption has been one of the most celebrated remediation technology in the treatment of wastewaters due to its simplicity, economy, high efficiency, flexibility, and recovery of ions based on the target pollutant and adsorbent that are employed [6].

Different types of adsorbents have been developed for the treatment of textile industrial effluents. Nanoparticles materials with ordered porosity and large surface area could serve as excellent candidates for the remediation of industrial wastewater. In this study, nanoparticles of alumina adsorbent were synthesized from kaolin. Very few reports are available on alumina synthesis from kaolin, and the ones we come across employed mixing of the surfactant with boehmite precursor after precipitation (*i.e*. in solid form). This resulted in a very weak interaction between the two; as such the surfactant has no significant role in the alumina synthesis and would result in non-ordered alumina with poor porosity. In this study, the surfactant was added to the solution of the boehmite precursor before its precipitation. Previously, none of the literature studies utilized polyoxyethylene (40) stearate as a surfactant. The utilization of kaolin in the alumina synthesis not only makes the process economical, but also makes it greener as the kaolin is locally available and environmentally benign, and the bi-product is silica, an economically viable product. Due to its physical, textural, thermal, and chemical properties, mesoporous γ-Al_2O_3 is an important material used as catalyst substrates and adsorbents. It is also used for the separation of large biological molecules and in environmental pollution control. The pore structural properties of mesoporous γ-alumina, high surface area and large pore volume, allows for the enhanced wastewater remediation. The goal of the present study is synthesis of organized mesoporous gamma-alumina, with improved structural properties, from local kaolin for enhanced treatment of dye-containing effluents by adsorption method.

EXPERIMENTAL

Materials

The kaolin was obtained from Getso town in Kano State, Nigeria. The hydrochloric acid and sodium hydroxide were purchased from QRëC^{TM}. The polyoxyethylene (40) stearate [poly(oxy-1,2-ethanediyl), alpha-hydro-omega-hydroxy-, octadecanoate] surfactant and Eriochrome Black T (EBT) dye were supplied by Sigma Aldrich. All reagents were of analytical grade and used without further purification.

Preparation of Adsorbent

The kaolin was calcined into metakaolin in a programmable furnace at 750 ºC for 3 h, at a heating rate of 5 °C min^{-1}. The metakaolin was leached with 6 M hydrochloric acid at 90 °C for 2 h under stirring at 600 rpm. Then an excess solution of 5 M NaOH was added to the filtered suspension to convert Al^{3+} into $NaAlO_2$ and precipitate metal ions impurities. To the solution of $NaAlO_2$, 20 ml of 0.45 g ml^{-1} polyoxyethylene (40) stearate (PS) was added and stirred for 30 min., and allowed to age for 2 days. The pH of the mixtures was then adjusted to 7 using 6 M HCl and 5 M NaOH solutions to precipitate boehmite. The precipitated boehmite was filtered, washed with deionized water, and dried at 110 ºC, followed by calcination at 500 ºC for 4 h. The alumina is known as Nano-Al [10] with modification.

Characterization

Structural phase analysis was carried out on a Bruker D8 having Siemens Diffractometer D5000 with Cu-Kα radiation (40 kV, 40 mA, λ = 1.5406 Å) (USA). Perkin Elmer 1650 Infra-Red Spectrometer (USA) was used for FTIR analysis in the range of 4000 cm^{-1} to 400 cm^{-1}. N_2 sorption was employed to determine the surface area, average pore diameter, and pore volume at -196 ºC using Fisher Thermo Scientific SURFER (USA). The morphology of the sample was obtained using field emission scanning electron microscopy analysis (FESEM) (Supra^{TM} 35 VP operating at 10 kV) (Germany). Finally, the chemical compositions were established using energy dispersive X-ray fluorescence spectrometer NEX CG (USA).

Preparation of Eriochrome Black T Dye

The Eriochrome Black T (EBT) dye stock solution was prepared by dissolving 1 g of the dye in a small amount of distilled water and made to mark in a 1000 ml volumetric flask. The working solutions and those for the calibration curve were prepared by diluting the stock solution in the appropriate proportion.

Batch Adsorption Study

The adsorption process was performed in a plastic sample bottle by collecting 100 ml of the dye solution of a specific concentration, adjusting the pH using 0.1 M solutions of NaOH and HCl, then adding a definite amount of the Nano-Al adsorbent, followed by shaking on a mechanical shaker for 30 minutes. At the end of the experiment, the dye solution was separated using Whatman No 42 filter paper and the absorbance was monitored using a Perkin Elmer UV-Vis spectrophotometer (Perkin Lambda) at a wavelength of 530 nm.

Statistical Analysis and Model Fitting

The adsorption parameters were optimized using response surface methodology (RSM) analysis applying a three-level factorial Central Composite design; the design factors were adsorbent loading, initial dye concentration, and pH of the adsorbate. Design-Expert 7.0 software was employed for the analysis. For predicting the optimal point, a second-order polynomial quadratic equation (Eq. (1)) was fitted to correlate the relationship between independent variables and responses and the interactive effect of the process variables. Regression coefficients of the quadratic model were evaluated by analysis of variance (ANOVA). All the terms in the model were tested by the student's F-test and the significance of the F-values at probability levels ($p \leq 0.05$) was analyzed. The developed mathematical models were used for the construction of three-dimensional (3D) response surface plots to predict the relationships between independent and dependent variables. The experimental data were evaluated with a determination coefficient (R^2), adjusted determination of coefficient (R^2 adj.), and predicted determination of coefficient (R^2 pred.).

$$Y = \lambda_o + \sum_{i=1}^{k} \lambda_i x_i + \sum_{i=1}^{k} \lambda_{ii} x_i^2 + \sum_{i=1}^{k} \sum_{j=i+1}^{k} \lambda_{ij} x_i x_j + \varepsilon \quad (1)$$

In Eq. (1), Y is the response, i and j are the linear and quadratic coefficients, respectively, k is the number of the studied and optimized factors in the experiment, λ is the regression coefficient, and ε is the arbitrary error [7].

The amount of EBT dye uptake by Nano-Al was calculated using Eq. (2);

$$q_e = \frac{(Co - Ce)V}{W} \quad (2)$$

Here, C_o is the initial concentration of adsorbate (mg l^{-1}), C_e is the final concentration of adsorbate (mg l^{-1}), W is the mass of adsorbent in gram (g), V is the volume of the adsorbate in a liter (l), and q_e is the adsorption capacity.

The adsorption efficiency can be expressed as the percentage removal of dye solution as shown in Eq. (3);

$$\text{Dye removal}\ (\%) = \frac{(Co - Ce)}{Co} \times 100 \quad (3)$$

RESULTS AND DISCUSSION

Adsorbent Characterization

X-Ray powder diffraction (XRD). The wide-angle diffractogram in Fig. 1 revealed characteristic peaks at 2θ = 32º 38º, 46º, and 67º assigned respectively to [2 2 0], [3 1 1], [4 0 0] and [4 4 0] crystal planes (JCPDS Card no 10-0425) for the Nano-Al sample. The broad peaks signify small crystallites with a small diameter [8].

Fourier transform infra-red spectroscopy (FTIR). The FTIR spectrum for the synthesized Nano-Al in Fig. 2 displays peaks around 3455, 2096, 1642, 1401, 767, and 579 cm^{-1}. The peaks at 3455 and 1642 cm^{-1} are attributed to the stretching and bending vibration of OH, respectively. While peak around 1401 cm^{-1} confirmed the formation of alumina [9,10]. Lastly, bands at 767 and 579 cm^{-1} are assigned to the AlO_4 and AlO_6, respectively.

Nitrogen adsorption-desorption analysis. From the N_2-sorption isotherms in Fig. 3, the Nano-Al sample exhibited type IV isotherm characteristic of mesoporous materials, the isotherm had an H4 hysteresis loop implying a slit-shaped pore [11]. Additionally, the isotherm revealed a narrow pore size distribution characteristic of ordered materials [12]. The narrow hysteresis loop implies the regularity of mesoporous alumina [13]. Moreover, the steepness of the adsorption

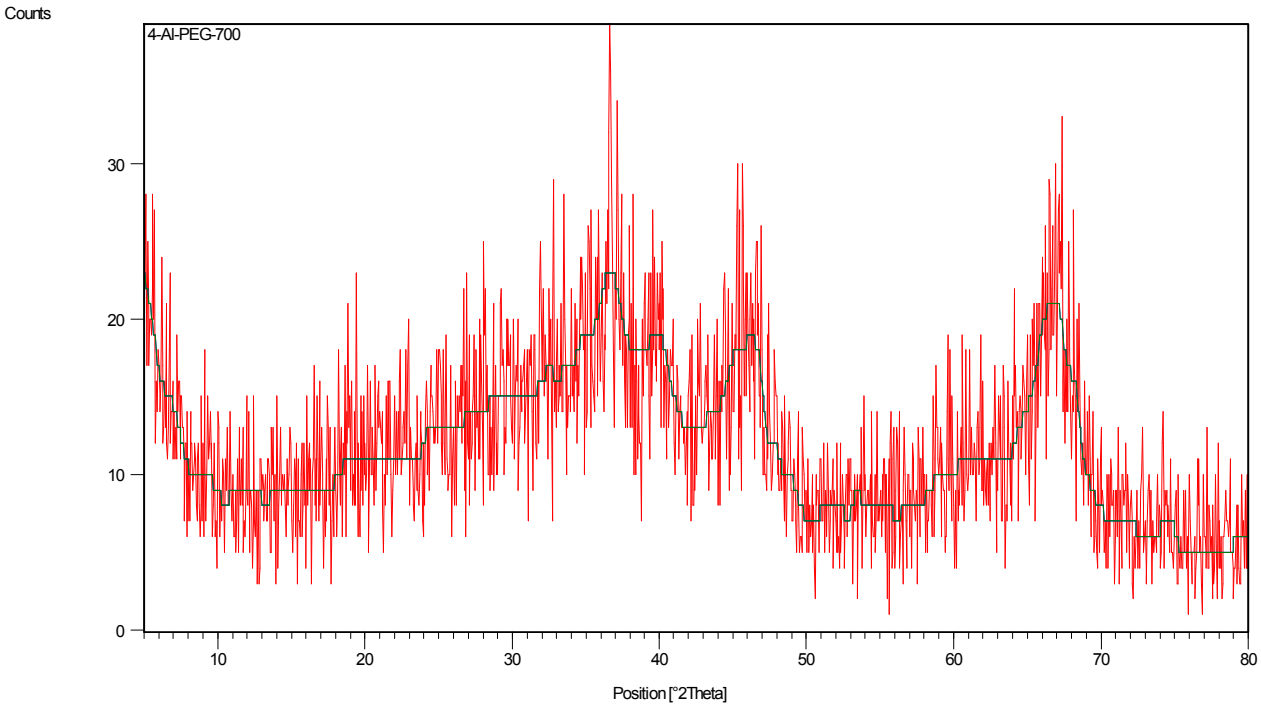

Fig. 1. XRD diffractogram of the Nano-Al.

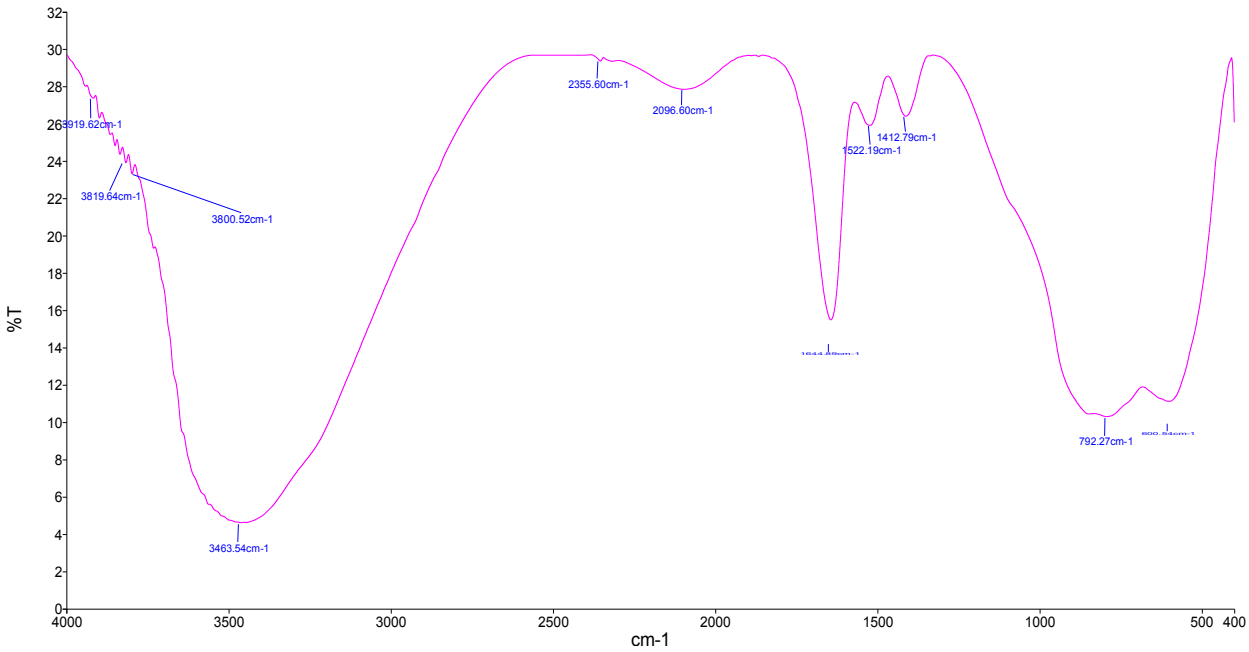

Fig. 2. FTIR spectrum of the Nano-Al.

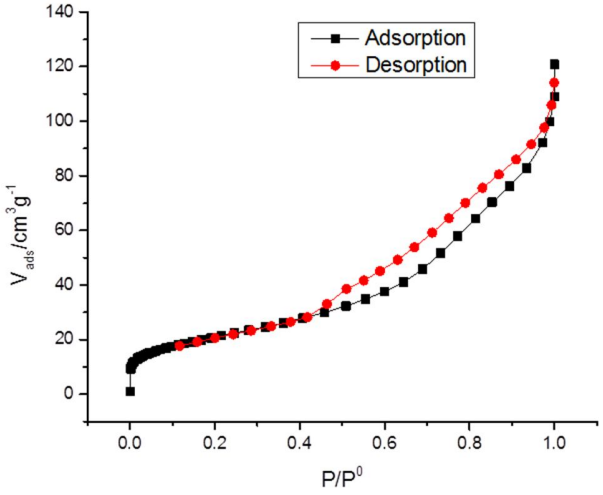

Fig. 3. N_2-sorption isotherm for the Nano-Al.

branch of the isotherms indicated an improved uniformity of mesopores [14]. This may be attributed to good interaction between the surfactant and boehmite precursor. The surface area, average pore diameter, and pore volume were found to be 76.0 m^2 g^{-1}, 4.4 nm, and 0.14 cm^3 g^{-1}, respectively. The low surface area is probably due to lower concentration of the surfactant than that of the critical micelles concentration (CMC). This can be true considering the unexpected large average pore diameter, which indicates the pore diameter assumed the size of the surfactant's molecules.

Field emission scanning electron microscopy (FESEM). The FESEM image of the Nano-Al sample depicted in Fig. 4 revealed a wormhole-like morphology. This signifies that the Nano-Al retained the wormhole-like structure of the boehmite, though, there is particle agglomeration.

X-Ray fluorescence (XRF). To ascertain the degree of purity of the alumina, an XRF analysis was performed. The Al_2O_3 composition in the Nano-Al sample was found to be 98%. This indicated the high purity of the synthesized Nano-Al, demonstrating the benefit of the introduction of the step for the precipitation of impurity in the synthesis procedure.

Response Surface Methodology

Three-level factorial Composite Design was applied for the RSM analysis, and the design factors were these: Adsorbent dosage (g) (A (0.5-2 g)), Initial dye concentration

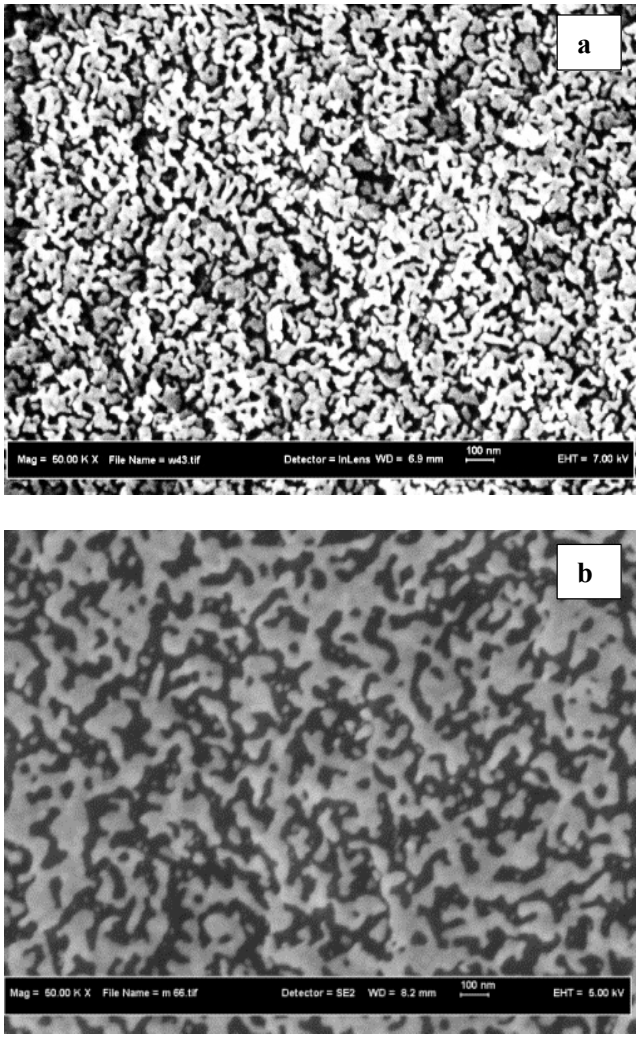

Fig. 4. FESEM images of a) boehmite precursor, b) Nano-Al.

(B (50-300 ppm)), and pH (C (3-10)). From the regression surface analysis and the analysis of variance (ANOVA), the second-order polynomial equation in terms of actual factors obtained from the multiple regression analysis of the experimental data that is expressed in Eqs. (4);

$$Y = 29.97 + 7.80 \times A - 5.42 \times B - 4.52 \times C - 1.78 \times A \times B + 2.05 \times A \times C - 4.73 \times B \times C + 7.33 \times A^2 + 17.76 \times B^2 + 25.47 \times C^2 \quad (4)$$

Here, Y is the response (*i.e.* % dye removal), while A, B, and C are the actual factors of the studied variables.

Table 1 shows the actual values of the reaction parameters and the responses obtained from the experiments conducted. While Table 2 is the result of ANOVA from the fitting of the experimental data to a second-order response surface model.

The results for the optimization of the adsorption of EBT dye on Nano-Al revealed a value of 0.8736 for the determination coefficient, indicating 87.36% of the dye removal could be due to the variation in the independent variables, whereas the remaining 12.64% of the response is due to residue. Additionally, an adequate precision of greater than 4 indicates the signal-to-noise ratio is adequate. Thus, the model can be used to navigate the design space. Furthermore, the "Lack of Fit F-value" of 1.44 suggests that it is not significant relative to the pure error, and there is a 34.93% chance that a "Lack of Fit F-value" this large could occur due to noise. This further ascertains the model's fit. The larger the F value, i.e. smaller Prob. > F, the higher the significance of the corresponding coefficient [15]. The Model F-value of 7.68 implies that the model is significant; hence, there is only a 0.19% chance that a "Model F-value" this large could occur due to noise. In this model, B^2 and C^2 are the most significant model terms. Thus, the most influential variables are the interaction between the initial dye concentration and itself, and that of pH with itself. Other moderately influential factors are adsorbent dosage, initial dye concentration, and pH. Their interactions are equally influential, but not to a large extent.

Generally, the result showed that the percentage adsorption of EBT increased with an increase in the adsorbent dosage, depending on the initial dye concentration and pH, and then it dropped after a certain limit was attained.

Table 1. Three-level Factorial Composite Design and the Response

Std.	Run	Block	Factor 1 A: Adsorbent dosage (g)	Factor 2 B: Initial concn. (ppm)	Factor 3 C: pH	Response 1 Percent dye removal (%)
14	1	Block 1	1.25	175.00	12.39	96.6
7	2	Block 1	0.50	300.00	10.00	60.7
8	3	Block 1	2.00	300.00	10.00	74
4	4	Block 1	2.00	300.00	3.00	86.7
9	5	Block 1	0.01	175.00	6.50	18.9
5	6	Block 1	0.50	50.00	10.00	84
20	7	Block 1	1.25	175.00	6.50	48.6
11	8	Block 1	1.25	35.22	6.50	85.7
19	9	Block 1	1.25	175.00	6.50	11.4
12	10	Block 1	1.25	385.22	6.50	63.6
15	11	Block 1	1.25	175.00	6.50	36.6
17	12	Block 1	1.25	175.00	6.50	19.4
3	13	Block 1	0.50	300.00	3.00	98.0
18	14	Block 1	1.25	175.00	6.50	31.4
1	15	Lock 1	0.50	50.00	3.00	86.0
6	16	Block 1	2.00	50.00	10.00	88
2	17	Block 1	2.00	50.00	3.00	98.2
13	18	Block 1	1.25	175.00	0.61	96.3
10	19	Block 1	2.51	175.00	6.50	71.4
16	20	Block 1	1.25	175.00	6.50	34.3

Table 2. Analysis of Variance (ANOVA) for the Quadratic Model

Source of variation	Quadratic sum of squares	Model degree of freedom (df)	Mean square	F-Values	P-Values Prob > F	Remark
Model	8487.69	9	1627.08	7.68	0.0019	Significant
A	350.29	1	830.43	3.92	0.0759	
B	2195.38	1	400.62	1.89	0.1990	
C	0.14	1	278.71	1.32	0.2780	
A^2	2291.05	1	774.46	3.66	0.0849	
B^2	49.79	1	4545.87	21.46	0.0009	
C^2	1149.20	1	9347.47	44.14	< 0.0001	
AB	1697.70	1	25.20	0.12	0.7373	
AC	4.96	1	33.62	0.16	0.6987	
BC	368.83	1	178.60	0.84	0.3801	
Residual	2474.14	10	211.79			
Lack of fit	1188.30	5	250.01	1.44	0.3493	Not significant
Pure error	1285.84	5	173.56			
Cor total	10961.83	19				

This is attributed to the fact that as the adsorbent dose is increased, the number of active sites for the dye sorption increases. This is followed by an overlap of active sorption sites with more adsorbent amounts, resulting in a little higher net number of available active sorption sites. Further increase in the adsorbent dosage appeared to congest the solution, resulting in the decrease of the adsorption [16].

The result also showed that the adsorption varied with the initial dye concentrations, depending on the remaining two parameters. The percent dye removal increased with initial dye concentration, and then dropped off when the concentration became so high. This is in line with the fact that the active sorption sites on the sorbent surface were saturated with adsorbed dye at high initial dye concentrations.

It is well known that the pH of the system is an important variable for the adsorption process in aqueous solutions. The adsorption process is primarily governed by the zero point charge (ZPC) of an adsorbent. Typically ZPC values for alumina fall within the range of pH 8-10, depending on the grades [17]. The alumina surface is positively charged below the ZPC and negatively charged above the ZPC. Accordingly, at pH below the ZPC, the adsorption sites on the surface of activated alumina adsorbs anionic species. The result of the adsorption of EBT onto the Nano-Al showed that the adsorption was favorable both under acidic and alkaline conditions, demonstrating its bi-functional nature. The percent dye removal was generally lower near-neutral pH. Consequently, the highest percent dye removal of 98.2% was obtained under these conditions: 2.00 g adsorbent dosage, 50 ppm initial dye concentration, and a pH of 3.00. Even though the Nano-Al had a small surface area, very high percentage dye removal was achieved. This may be attributed to the enhanced structural properties of the Nano-Al.

Sorption Isotherms

The pattern of EBT sorption onto Nano-Al at equilibrium relative to the equilibrium concentration was studied using Langmuir, Freundlich, and Temkin isotherms. The Langmuir isotherm assumes monolayer coverage of adsorbent that occurs over specific homogenous sites on the adsorbent, while the Freundlich isotherm allows for multisite adsorption onto a heterogeneous surface, and the Temkin isotherm model contains a factor that explicitly takes into account the interactions between adsorbate and adsorbent species [18]. It presumes that the heat of adsorption of all the molecules in the layer decreases linearly with the coverage involved in this

interaction.

The linear form of Langmuir isotherm in Eq. (5) was used for appraising its applicability to the sorption data [19,20].

$$\frac{C_e}{q_e} = \frac{1}{K_L} + \frac{a_L}{K_L} C_e \quad (5)$$

Here, q_e is the amount adsorbed per specified amount of adsorbent (mg g^{-1}), C_e is the equilibrium concentration (mg l^{-1}), while K_L (l g^{-1}), and a_L (l mg^{-1}) are the adsorption equilibrium constant. A plot of C_e/q_e *versus* C_e in Fig. 5 gives a straight line with a high correlation coefficient of 0.924, which implies the Langmuir model is a good fit for the Nano-Al-EBT system. The theoretical monolayer capacity Q_m is numerically equal to K_L/a_L. The values of K_L, a_L, and Q_m are presented in Table 3.

Furthermore, the favorability of adsorption of EBT described by the Langmuir isotherm model was estimated using the dimensionless separation factor (R_L). The expression for R_L is given in Eq. (6); it is an essential feature of the Langmuir model [21].

$$R_L = \frac{1}{(1+K_L C_0)} \quad (6)$$

Here, K_L (l mg^{-1}) is the equilibrium constant obtained from Langmuir isotherm while C_0 (mg l^{-1}) is the initial adsorbate concentration.

The value for R_L of 0.00068 indicates the Langmuir isotherm is favorable, since the shape of the isotherm is considered unfavorable if $R_L > 1$, linear if $R_L = 1$, and favorable if $0 < R_L < 1$ [21].

To assess the possibility of multisite adsorption of EBT onto Nano-Al surface, the linear form of Freundlich isotherm in Eq. (7) was employed.

$$\log q_e = \log K_F + \frac{1}{n} \log C_e \quad (7)$$

Here, K_F [mg g^{-1} (l $mg^{-1})^{1/n}$] is roughly an indicator of the sorption capacity as well as the strength of the adsorptive bond, and n is the heterogeneity factor that represents the bond distribution. Both K_F and n are Freundlich constants whose values depend on experimental conditions. When $1/n$ is much less than 1, the adsorbent is said to be heterogeneous [16,22]. As can be observed, the Freundlich plot of $\log q_e$

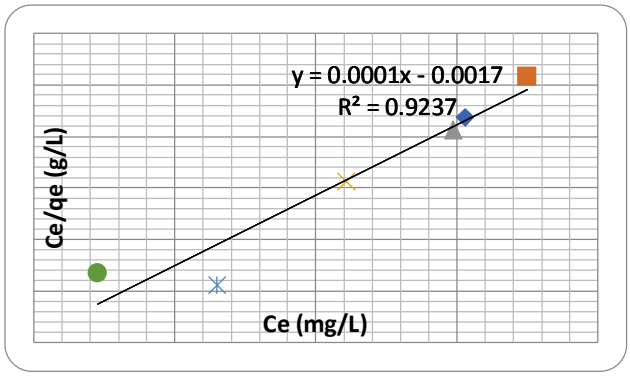

Fig. 5. Langmuir isotherm plot.

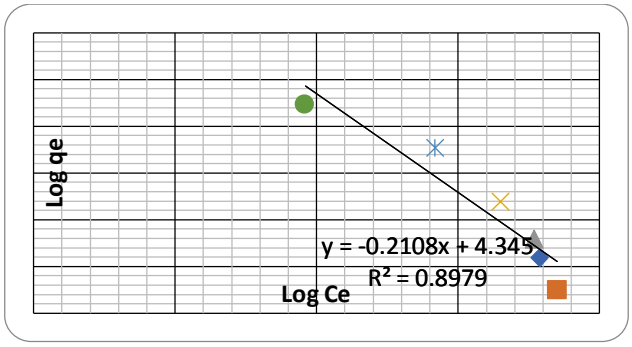

Fig. 6. Freundlich isotherm plot.

against $\log C_e$ in Fig. 6 gave a straight line with an R^2 value of 0.898. Thus, the model is considered not a very much fit for the data.

Lastly, the linear form of the Temkin model as expressed in Eq. (8) was also tested for the sorption data.

$$q_e = B\, In\, K_T + B\, In\, C_e \quad (8)$$

Where,

$$B = \frac{RT}{b} \quad (9)$$

Here, K_T is the Temkin equilibrium binding constant (l mg^{-1}) corresponding to maximum binding energy, and a constant B is related to the heat of adsorption [19]. A plot of q_e *vs.* $\ln C_e$ in Fig. 7 showed a linear line with an R^2 value of 0.879. This suggests that the model fits the experimental data to a small extent. Consequently, Langmuir isotherm is the best fit for the sorption data, which implies monolayer sorption of EBT

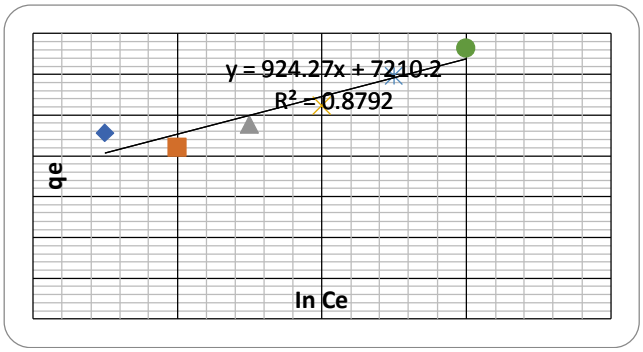

Fig. 7. Temkin isotherm plot.

onto the Nano-Al. Table 3 shows the summary of the isotherms models' parameters for the adsorption data.

Adsorption Kinetics

To evaluate the kinetics order of the sorption process, the Lagergren pseudo-first-order and the pseudo-second-order models were tested for the sorption process. The linear form of the Lagergren pseudo-first-order expression in Eq. (9) was employed.

$$\log(q_e - q_t) = -\frac{k_1}{2.303}t + \log q_e \qquad (9)$$

Here, q_t (mg g^{-1}) is the concentration at any time t, q_e (mg g^{-1}) is the maximum sorption capacity of the pseudo-first-order, and k_1 (min^{-1}) is the pseudo-first-order rate constant. However, the non-linear nature of the plot of log(q_e - q_t) *vs.* t indicates that the sorption process does not fit the kinetic model.

Hence, the linear form of the pseudo-second-order as expressed in Eq. (10) was tested for the sorption kinetics.

$$\frac{t}{q_t} = \frac{1}{k_2 q_e^2} + \frac{t}{q_e} \qquad (10)$$

Where; q_t (mg g^{-1}) is the dye concentration at any time t, q_e (mg g^{-1}) is the maximum sorption capacity of the pseudo-second-order, and k_2 (g (mg^{-1} min^{-1})) is the rate constant. Plotting t/q_t *vs.* time t gave a straight line as shown in Fig. 8. The plot has a very high R^2 value of 0.940, indicating a very good fit for the model. This implies that the pseudo-second-order model is the appropriate kinetic model to describe the sorption kinetics. The pseudo-second-order model has been

Table 3. Adsorption Isotherms Models' Parameters

Langmuir adsorption isotherm	
K_L (l g^{-1})	8.403
a_L (l mg^{-1})	8.143
Q_m (mg g^{-1})	1.032
R^2	0.923
Freundlich adsorption isotherm	
K_F (l mg^{-1})	22.130
n	4.762
R^2	0.897
Temkin adsorption isotherm	
K_T (l mg^{-1})	2.444
B (J mol^{-1})	924.2
R^2	0.879

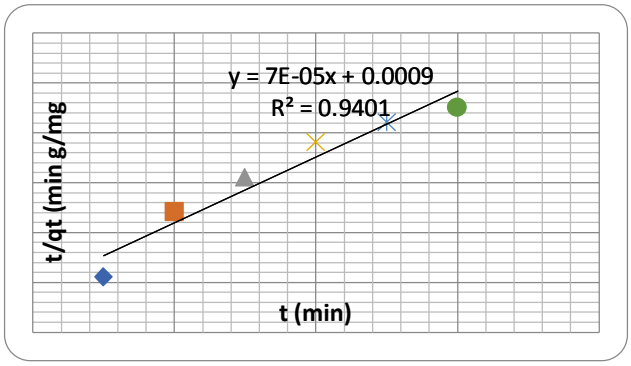

Fig. 8. Pseudo-second-order plot.

reported as the most suitable for describing ionic-type adsorption; this means the EBT absorption is governed by the chemisorption process. The model's fit is further buttressed by the agreement between the calculated and the experimental q_e values of 14.29 mg g^{-1} and 13.27 mg g^{-1}, respectively [17].

Sorption Mechanism

The adsorption process is governed by external mass transfer, intra-particle diffusion, or a combination of the two, *i.e.* solute transfer processes [19]. The model developed previously [23], presented in Eq. (11), has been used to

evaluate the possibility of intra-particle diffusion as the sorption rate controlling mechanism in the adsorption process. The model assumes that migration of adsorbate through the pores of the adsorbent can be an adsorption rate-limiting step if there is some strain for the migration of the adsorbate through the adsorbent surface due to adsorbent size.

$$q_t = k_{id} t^{1/2} + I \quad (11)$$

In Eq. (11), k_{id} is the intra-particle diffusion rate constant (mg (g^{-1} $min^{-1/2}$)), and I (mg g^{-1}) is the intercept that reflects the thickness of the boundary layer. For the intra-particle diffusion to be the sorption rate-controlling step, the plot of q_t *vs.* $t^{1/2}$ has to be linear passing the origin [24]. Conversely, the plot in Fig. 9 does not pass through the origin and has an R^2 value of 0.879. This indicates that intra-particle diffusion is not the only rate-controlling factor. Thus, more than one process affects the adsorption process. But, the large I value of 7210 mg g^{-1} implies a greater contribution of the surface sorption in the rate-controlling step [24].

Consequently, the likelihood of external diffusion contributing to the sorption rate-controlling step is evaluated using the diffusion model depicted in Eq. (12) [16].

$$In\frac{C_t}{C_0} = -k_f \frac{A}{V} t \quad (12)$$

Here, C_0 (mg l^{-1}) is the initial dye concentration, C_t (mg l^{-1}) is the dye concentration at time t, A/V is the external adsorption area to the total solution volume, t is the adsorption time, and k_f is the external diffusion coefficient. Similarly, for the external diffusion to be the sorption rate-controlling process, the plot of $\ln C_t/C_0$ against t should be linear. However, the non-linear nature of the plot in Fig. 10 over the whole time range confirms that intra-particle diffusion is the major rate-controlling factor with little contribution from external diffusion.

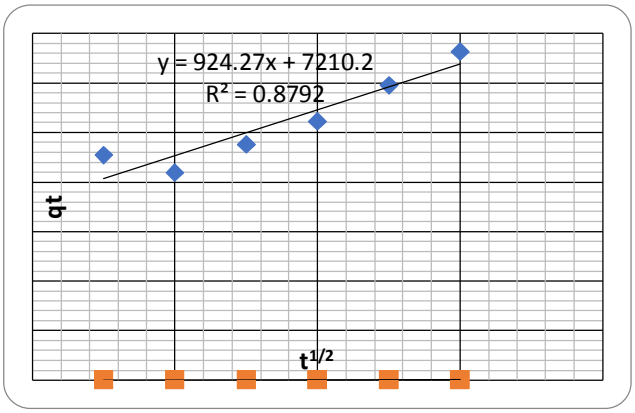

Fig. 9. Intra-particle diffusion plot.

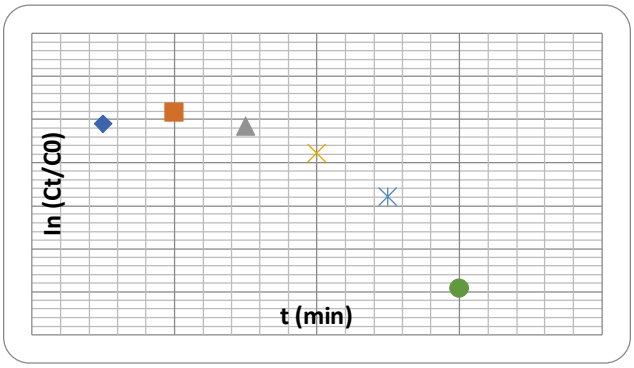

Fig. 10. External diffusion plot.

CONCLUSIONS

Alumina (Al_2O_3) nanoparticles with ordered mesoporosity, good crystallinity, and moderate surface area were synthesized from local kaolin. The FTIR analysis of the alumina indicated that it possessed both tetrahedral and octahedral structures. The N_2-sorption study revealed respective surface area, average pore diameter, and pore volume of 76.0 m^2 g^{-1}, 4.4 nm, and 0.14 cm^3 g^{-1}. Also, the morphology of the alumina nanoparticles was wormhole-like, and it had up to 98% Al_2O_3 composition. The alumina (Nano-Al) was applied for the adsorption of EBT dye, and the process was optimized using RSM analysis by the Central Composite Design model. From the optimization result the interactions between initial dye concentration and itself, and that of pH with itself were found to be the most influential on the adsorption process, followed by adsorbent dosage, initial dye concentration, and then pH. The R^2 (0.8736) of the model implies that 87.36% of the percentage dye removal could be due to the variation in the independent variable. Accordingly, up to 98.2%, dye removal was achieved at pH of 3, adsorbent dosage (2.0 g), and initial dye concentration (50 ppm). This

is despite the small surface area of the Nano-Al. Hence, the high percentage dye removal was attributed to the enhanced structural properties of the Nano-Al. From the sorption and kinetics data, the adsorption process was best fitted to the Langmuir isotherm and pseudo-second-order model.

ACKNOWLEDGMENTS

The authors earnestly acknowledge the Tertiary Education Trust Fund (TETFund), Nigeria under Institutional Based Research (IBR) funds for the financial support.

REFERENCES

[1] Medjor, W. O.; Akpoveta, V. O.; Egharevba, F., Kinetics and Physicochemical Studies of Surfactant Enhanced Remediation of Hydrocarbons Contaminated Groundwater, *EJPE*, **2018**, *27*(2), 169-176, DOI: 10.1016/j.ejpe.2017.02.005.

[2] Senthilkumaar, C. V.; Kalaamani, S.; Porkodi, P.; Varadarajan, K.; Subburaam, P. R., Adsorption of Dissolved Reactive Red Dye Fromaqueous Phase onto Activated Carbon Prepared from Agricultural Waste, *Bioresour. Technol.*, **2006**, *97*, 1618-1625, DOI: 10.1016/j.biotech.2005.08.001.

[3] Gupta, V. K.; Ali, V. K.; Saini, I., Adsorption Studies on the Removal of Vertigo Blue 49 and Orange DNA1$_3$ from Aqueous Solutions Using Carbon Slurry Developed from a Waste Material, *J. Colloid Interface Sci.*, **2007**, *315*, 87-93, DOI: 10.1016/j.jcis.2007.06.063.

[4] El Qada, G. M.; Allen, E. N.; Walker, S. J., Adsorption of Methylene Blue onto Activated Carbon Produced from Steam Activated Bituminous Coal: A Study of Equilibrium Adsorption Isotherm, *Chem. Eng. J.*, **2006**, *124*, 103-110, DOI: 10.1016/j.cej.2006.08.015.

[5] Azmier, M.; Azreen, N.; Puad, A.; Solomon, O., Kinetic, Equilibrium and Thermodynamic Studies of Synthetic Dye Removal Using Pomegranate Peel Activated Carbon Prepared by Microwave-induced KOH Activation, *WRI*, **2014**, *6*, 18-35, DOI: 10.1016/j.wri.2014.06.002.

[6] Olaoye, H. G.; Afolayan, R. A.; Mustapha, O. D.; Adeleke, O. I., The Efficacy of Banana Peel Activated Carbon in the Removal of Cyanide and Selected Metals from Cassava Processing Wastewater., *AIR*, **2018**, *16*(1), 1-12, DOI: 10.9734/AIR/2018/43070.

[7] Badday, A. S.; Abdullah, A. Z.; Lee, K., Optimization of Biodiesel Production Process from Jatropha Oil Using Supported Heteropolyacid Catalyst and Assisted by Ultrasonic Energy, *Renew. Energy*, **2013**, *50*, 427-432, DOI: 10.1016/j.renene.2012.07.013.

[8] Khosravi, M.; Baiyu, M.; Calvin, H., Synthesis and Characterization of Silica Doped Alumina Catalyst Support with Superior Thermal Stability and Unique Pore Properties, *J. Porous Mater.*, **2016**, *23*(2), 475-487, DOI: 10.1007/s10934-015-0101-z.

[9] Yang, H.; Liu, M.; Ouyang, J., Novel Synthesis and Characterization of Nanosised γ-Al_2O_3 from Kaolin, *Appl. Clay Sci.*, **2010**, *47*, 438-443, DOI: 10.1016/j.clay.2009.12.021.

[10] Pan, F. L.; Wang, X.; Wang, T.; Zhang, Yun.; Yan, Z.; Yang, Y. S., Synthesis of Large-mesoporous γ-Al_2O_3 from Coal-series Kaolin at Room Temperature, *Mater. Lett.*, **2013**, *91*(1), 136-138, DOI: 10.1016/j.matlet.2012.09.052.

[11] Rouquerol, F.; Rouquerol, J.; Sing, K. S.; Llewellyn, W.; Maurin, G., Adsorption by Powders and Porous Solids. Principles, Methodology and Application, Second Ed. The Boulevard, Langford Lane, Kidlington, Oxford OX5 1GB, UK Radarweg 29, **2014**.

[12] Lesaint, C.; Kleppa, G.; Arla, D.; Glomm, W. R.; Øye, G., Synthesis and Characterization of Mesoporous Alumina Materials with Large Pore Size Prepared by a Double Hydrolysis Route, *Microporous. Mesoporous. Mater.*, **2009**, *119*(1-3), 245-251, DOI: 10.1016/j.micromeso.2008.10.022.

[13] Valange, S.; Guth, J. L.; Kolenda, F.; Lacombe, S.; Gabelica, Z., Synthesis Strategies Leading to Surfactant-assisted Aluminas with Controlled Mesoporosity in Aqueous Media, Microporous. *Mesoporous. Mater.*, **2000**, *35-36*, 597-607, DOI: 10.1016/S1387-1811(99)00253-X.

[14] Zhang, W.; Zheng, X.; Zhao, X.; Zheng, Y.; Jiang, L., Carboxylic Acid Assisted Synthesis of Ordered Mesoporous Silicon-doped γ-Alumina with High Thermal Stability, *Mater. Lett.*, **2015**, *160*, 85-87, DOI: 10.1016/j.matlet.2015.07.097.

[15] Goupy, J.; Lee, C., Introduction to Design of Experiments With JMP Examples, 3rd Edition. SAS Institute Inc., Cary, NC, USA, **2007**.

[16] Gitari, W. M.; Izuagie, A. A.; Gumbo, J. R., Synthesis, Characterization and Batch Assessment of Groundwater Fluoride Removal Capacity of Trimetal Mg/Ce/Mn Oxide-modified Diatomaceous Earth, *Arab. J. Chem*., 2020, *13*(1), 1-16, DOI: 10.1016/j.arabjc.2017.01.002.

[17] Lee, G.; Chen, C.; Yang, S.; Ahn, W., Enhanced Adsorptive Removal of Fluoride Using Mesoporous Alumina, *Microporous. Mesoporous. Mater*., **2010**, *127*(1-2), 152-156, DOI: 10.1016/j.micromeso.2009.07.007.

[18] Temkin, V.; Pyzhev, M. J., Recent Modifications to Langmuir Isotherms.," Acta Physiochim. USSR, **1940**, *12*, 217.

[19] Banerjee, S.; Chattopadhyaya, M. C., Adsorption Characteristics for the Removal of a Toxic Dye, Tartrazine from Aqueous Solutions by a Low Cost Agricultural by-Product, *Arab. J. Chem*., **2017**, *10*, S1629-S1638, DOI: 10.1016/j.arabjc.2013.06.005.

[20] Ali, A.; Saeed, K.; Mabood, F., Removal of Chromium (VI) from Aqueous Medium Using Chemically Modified Banana Peels as Efficient Low-cost Adsorbent, *AEJ*, **2016**, *55*(3), 2933-2942, DOI: 10.1016/j.aej.2016.05.011.

[21] Weber, R. K.; Chakravorti, T. W., Pore and Solid Diffusion Models for Fixed Bed Adsorbents., *AIChE J*., **1974**, *20*, 228-238, DOI: 10.1002/aic.690200204.

[22] Panda, H.; Tiadi, N.; Mohanty, M.; Mohanty, C. R., Studies on Adsorption Behavior of an Industrial Waste for Removal of Chromium from Aqueous Solution, *SAJCE*, **2017**, *23*, 132-138, DOI: 10.1016/j.sajce.2017.05.002.

[23] Weber Jr., J. C.; Morris, W. J., Kinetics of Adsorption on Carbon from Solution.," *J. Sanit. Eng. Div. Proc. Am. Soc. Civ. Eng*., **1963**, *89*, 31. DOI: ?

[24] Inyinbor, A. A.; Adekola, F. A.; Olatunji, G. A., Kinetics, Isotherms and Thermodynamic Modeling of Liquid Phase Adsorption of Rhodamine B Dye onto Raphia Hookerie Fruit Epicarp, *WRI*, **2016**, *15*, 14-27, DOI: 10.1016/j.wri.2016.06.001.